1.5 Solving the evolution equations

The evolution basis, numerical solution in x and in moment space, heavy-quark thresholds, and the behaviour at large and small x.

1. What has to be solved

Chapter 1.4 derived the DGLAP equations. For n_f quark flavours they are $2n_f + 1$ coupled integro-differential equations, one for each quark, each antiquark and the gluon. Chapter 1.4 also solved the simplest cases at leading order: one moment of a non-singlet distribution, Eq. (1.4.28), and the eigenvalues of the singlet system, Eq. (1.4.29).

This chapter turns those results into a working method. A fit needs the distributions at the scale of every data point, starting from a parametrisation at one scale Q_0. The chapter establishes five things.

1. **A change of basis reduces the problem** to one coupled pair of equations and a list of single equations. The basis is written out in full, with the rotation matrix and its inverse (section 2).
2. **Evolution is a linear map.** It can be computed once, stored as a matrix, and combined with the hard cross-section into an FK table. This is why a fit is fast (section 3).
3. **There are two ways to compute the map.** One works in moment space, where the leading-order solution is exact (sections 4 and 5). The other works on a grid in x (section 6). Both are implemented in this chapter's check script, and they agree to the accuracy stated in section 6.
4. **The number of flavours changes with the scale.** Each heavy quark switches on at its mass, and the distributions on the two sides of a threshold have to be matched (section 7).
5. **The solution has simple limits** at large x and at small x, and the small-x limit marks where the fixed-order equations stop being reliable (sections 8 and 9).

The chapter follows Ellis, Stirling and Webber (ESW), sections 4.3.3, 4.3.4 and 4.6 [1], and Moore's thesis, sections 1.2.1 and 1.2.4 [2]. Throughout, $t = \ln \mu^2$ is the evolution variable, α_S the strong coupling, and

$$\zeta = \ln \frac{\alpha_S(\mu_0^2)}{\alpha_S(\mu^2)}$$

is the leading-order evolution "time" that appeared in the exponent of Eq. (1.4.28). It is zero at $\mu = \mu_0$ and grows like $\ln \ln \mu^2$.

2. The evolution basis

This section constructs the combinations of quark distributions that evolve independently, and gives the explicit map between them and the individual flavours.

Sums and differences of quark and antiquark

For each flavour i define

$$q_i^{\pm}(x, \mu^2) = q_i(x, \mu^2) \pm \bar{q}_i(x, \mu^2). \tag{1.5.1}$$

q_i^- is the valence distribution of flavour i: its integral over x counts quarks minus antiquarks. q_i^+ is the total quark-plus-antiquark content. Deep inelastic scattering through a photon measures the q_i^+, because the squared charge is the same for a quark and its antiquark.

The flavour structure of the kernels

A gluon is flavour-blind, and QCD treats all massless flavours alike. The kernel that takes a quark of flavour k to a quark of flavour i can therefore have only two parts: one that requires $i = k$, and one that is the same for every pair of flavours. With the same split for quark to antiquark (ESW Eq. 4.95):

$$P_{q_i q_k} = \delta_{ik}\, P_{qq}^V + P_{qq}^S, \qquad P_{q_i \bar{q}_k} = \delta_{ik}\, P_{q\bar{q}}^V + P_{q\bar{q}}^S. \tag{1.5.2}$$

In the δ_{ik} parts the quark line runs through from parent to daughter. The P^S parts need the parent quark to turn into a gluon that then makes a new pair, so they start at order α_S^2, as does $P_{q\bar{q}}^V$. At leading order $P_{qq}^V = P_{qq}^{(0)}$ of Eq. (1.4.21) and the other three vanish. Charge conjugation gives the antiquark kernels: $P_{\bar{q}_i \bar{q}_k} = P_{q_i q_k}$ and $P_{\bar{q}_i q_k} = P_{q_i \bar{q}_k}$.

Inserting Eq. (1.5.2) into the general evolution equations and taking the sum and the difference of the quark and antiquark equations gives (derivation D1)

$$\begin{aligned} \frac{\partial q_i^+}{\partial t} &= \frac{\alpha_S}{2\pi}\Big[P^+ \otimes q_i^+ + \big(P_{qq}^S + P_{q\bar{q}}^S\big) \otimes \Sigma + 2P_{qg} \otimes g\Big], \\ \frac{\partial q_i^-}{\partial t} &= \frac{\alpha_S}{2\pi}\Big[P^- \otimes q_i^- + \big(P_{qq}^S - P_{q\bar{q}}^S\big) \otimes V\Big], \end{aligned} \qquad P^\pm = P_{qq}^V \pm P_{q\bar{q}}^V. \tag{1.5.3}$$

Here $\Sigma = \sum_i q_i^+$ is the singlet and $V = \sum_i q_i^-$ is the total valence. The structure is now visible. The terms that couple different flavours, and the gluon term, are the same for every i. They cancel in any difference of two q^+ or of two q^-.

The non-singlet combinations

Choose the differences as follows (ESW Eq. 4.97, in the labelling used by NNPDF and Colibri):

$$\begin{aligned} T_3 &= u^+ - d^+, & V_3 &= u^- - d^-, \\ T_8 &= u^+ + d^+ - 2s^+, & V_8 &= u^- + d^- - 2s^-, \\ T_{15} &= u^+ + d^+ + s^+ - 3c^+, & V_{15} &= u^- + d^- + s^- - 3c^-, \\ T_{24} &= u^+ + d^+ + s^+ + c^+ - 4b^+, & V_{24} &= u^- + \cdots + c^- - 4b^-, \\ T_{35} &= u^+ + d^+ + s^+ + c^+ + b^+ - 5t^+, & V_{35} &= u^- + \cdots + b^- - 5t^-. \end{aligned} \tag{1.5.4}$$

The pattern is: the sum of the first $n-1$ flavours minus $n-1$ times the n-th, labelled by $n^2 - 1$. Each is a sum of differences of pairs, so the common terms in Eq. (1.5.3) drop out, and each obeys a single closed equation:

$$\frac{\partial T_j}{\partial t} = \frac{\alpha_S}{2\pi}\, P^+ \otimes T_j, \qquad \frac{\partial V_j}{\partial t} = \frac{\alpha_S}{2\pi}\, P^- \otimes V_j, \qquad \frac{\partial V}{\partial t} = \frac{\alpha_S}{2\pi}\, P^V \otimes V, \tag{1.5.5}$$

with $P^V = P^- + n_f\,(P_{qq}^S - P_{q\bar{q}}^S)$. Summing the first line of Eq. (1.5.3) over flavours gives the singlet equation (1.4.23), with $P_{qq} = P^+ + n_f\,(P_{qq}^S + P_{q\bar{q}}^S)$ (ESW Eq. 4.101).

Three remarks.

- **At leading order all the non-singlet kernels are the same**, $P^+ = P^- = P^V = P_{qq}^{(0)}$, and every non-singlet moment evolves by Eq. (1.4.28).

- **At next-to-leading order** $P^+ \neq P^-$, because $P^V_{q\bar{q}}$ is no longer zero. ESW give both functions in their Eqs. (4.107) and (4.108). At this order $P^S_{qq} = P^S_{q\bar{q}}$ (ESW Eq. 4.96), so $P^V = P^-$.
- **From next-to-next-to-leading order** $P^V \neq P^-$, which is the third non-singlet kernel mentioned in chapter 1.4. This is the reason the total valence V is kept as its own basis element and not folded into the V_j.

The singlet Σ is the one quark combination in which the common terms add up instead of cancelling, so it stays coupled to the gluon.

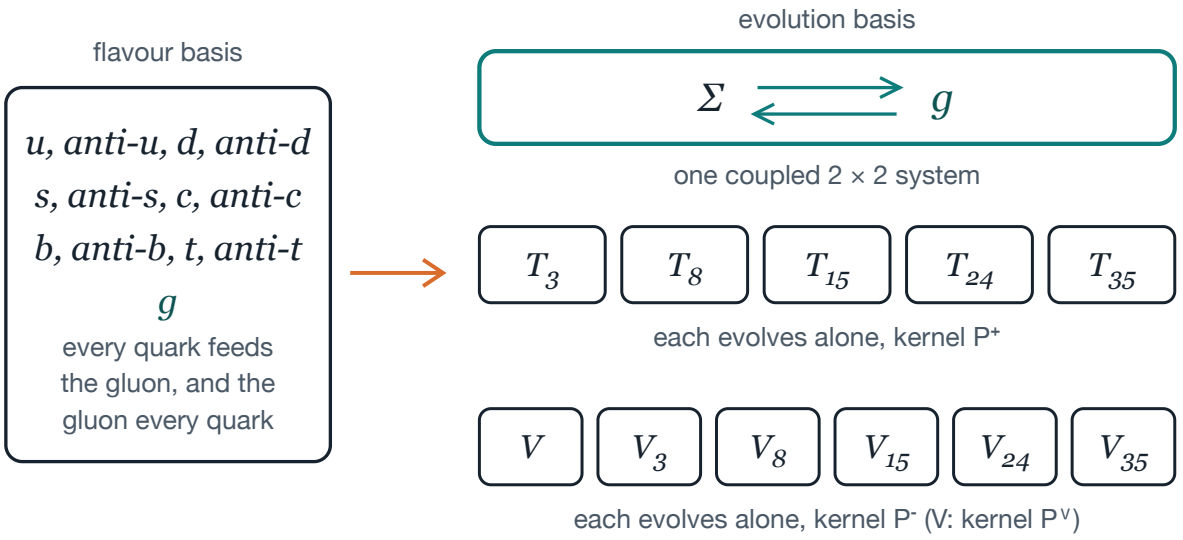

Figure 1. The change of basis. On the left, thirteen distributions in which every quark is coupled to the gluon and, beyond leading order, to every other quark. On the right, the same information arranged so that only Σ and g are coupled. The other eleven combinations each obey a single equation of the form (1.5.5). With the photon, which is switched off in our fits, these are the fourteen components of the basis used by NNPDF and Colibri.

The rotation for the light flavours

With three flavours the quark part of the map is a 6×6 matrix. Ordering the flavour basis as $(u, \bar{u}, d, \bar{d}, s, \bar{s})$:

$$\begin{pmatrix} \Sigma \\ V \\ V_3 \\ V_8 \\ T_3 \\ T_8 \end{pmatrix} = R \begin{pmatrix} u \\ \bar{u} \\ d \\ \bar{d} \\ s \\ \bar{s} \end{pmatrix}, \qquad R = \begin{pmatrix} 1 & 1 & 1 & 1 & 1 & 1 \\ 1 & -1 & 1 & -1 & 1 & -1 \\ 1 & -1 & -1 & 1 & 0 & 0 \\ 1 & -1 & 1 & -1 & -2 & 2 \\ 1 & 1 & -1 & -1 & 0 & 0 \\ 1 & 1 & 1 & 1 & -2 & -2 \end{pmatrix}. \tag{1.5.6}$$

The rows of R are mutually orthogonal, with squared lengths $6, 6, 4, 12, 4, 12$. So RR^T is the diagonal matrix D of those numbers, and the inverse needs no computation: $R^{-1} = R^T D^{-1}$. Written out,

$$\begin{aligned} u,\ \bar{u} &= \tfrac{1}{12}\big[2\Sigma + 3T_3 + T_8 \pm (2V + 3V_3 + V_8)\big], \\ d,\ \bar{d} &= \tfrac{1}{12}\big[2\Sigma - 3T_3 + T_8 \pm (2V - 3V_3 + V_8)\big], \\ s,\ \bar{s} &= \tfrac{1}{6}\big[\Sigma - T_8 \pm (V - V_8)\big], \end{aligned} \tag{1.5.7}$$

with the upper sign for the quark. The same holds with all six flavours: the twelve rows built from Eq. (1.5.4) are orthogonal, with squared lengths 12 for Σ and V and $2n(n-1)$ for the combinations labelled $n^2 - 1$.

Two uses of these formulas matter later.

A structure function in the evolution basis. For three flavours the parton-model F_2 of Eq. (1.4.1) is $x\big[\frac{4}{9}u^+ + \frac{1}{9}d^+ + \frac{1}{9}s^+\big]$. Substituting Eq. (1.5.7):

$$F_2^p = x\Big[\tfrac{2}{9}\,\Sigma + \tfrac{1}{6}\,T_3 + \tfrac{1}{18}\,T_8\Big], \qquad F_2^p - F_2^n = \tfrac{1}{3}\,x\,T_3. \tag{1.5.8}$$

The second relation uses isospin symmetry, under which the neutron is the proton with u and d exchanged. The difference between proton and neutron targets is carried entirely by T_3.

Absent heavy quarks. If the proton contains no charm at some scale, $c^+ = c^- = 0$, then Eq. (1.5.4) gives $T_{15} = \Sigma$ and $V_{15} = V$ there. The same holds for T_{24}, T_{35} and V_{24}, V_{35} when bottom and top are absent. A model that describes only light quarks therefore still fills all fourteen components. It sets the heavy ones equal to Σ or V, not to zero.

---

3. The evolution operator

This section shows that evolution from one scale to another is a fixed linear map, and that on a grid in x the map is a matrix that can be computed once.

Linearity

The DGLAP equations are linear and homogeneous in the distributions. The sum of two solutions is a solution, and a solution multiplied by a constant is a solution. The solution at Q^2 is therefore a linear functional of the input at Q_0^2. Collect the distributions into a vector f_a, with a running over the components of the evolution basis. Then

$$f_a(x, Q^2) = \sum_b \int_0^1 dy\; E_{ab}(x, y; Q^2, Q_0^2)\, f_b(y, Q_0^2). \tag{1.5.9}$$

E is the *evolution operator*. It depends on the two scales, on the perturbative order, on α_S and on the quark masses. It does not depend on the distributions it acts on. Three of its properties follow from the equations.

$$\begin{aligned} E(Q_0^2, Q_0^2) &= 1, \\ E(Q_2^2, Q_0^2) &= E(Q_2^2, Q_1^2)\, E(Q_1^2, Q_0^2), \\ E_{ab}(x, y) &= 0 \quad \text{for } y < x. \end{aligned} \tag{1.5.10}$$

The first says that no evolution happens over zero distance. The second says that evolving to Q_1 and then on to Q_2 is the same as evolving directly; the product includes the sum over components and the integral over the intermediate momentum fraction. The third is the statement from chapter 1.4 that a parton at x can only have come from a parent with more momentum.

In the evolution basis E is block diagonal: a 2×2 block for (Σ, g) and a single entry for each non-singlet. Because the convolution in Eq. (1.4.19) depends on x and y only through x/y, so does the operator: $E(x, y) = \Gamma(x/y)/y$ for some function Γ. Its Mellin transform is what chapter 1.4 already computed. For a non-singlet at leading order it is $\big[\alpha_S(Q_0^2)/\alpha_S(Q^2)\big]^{d_{qq}(N)}$, Eq. (1.4.28).

A matrix on a grid

A computer stores a distribution as its values at a set of nodes $x_1 < x_2 < \cdots < x_n$. Between the nodes it is reconstructed by interpolation:

$$x\, f_b(x, Q_0^2) \;\approx\; \sum_{k=1}^{n} w_k(x)\; x_k\, f_b(x_k, Q_0^2). \tag{1.5.11}$$

The w_k are fixed interpolating functions with $w_k(x_j) = \delta_{jk}$, each non-zero only near its own node. Substituting into Eq. (1.5.9) and evaluating the result at the nodes turns the integral operator into a matrix $E_{aj,bk}$ with one index pair for the output (component a, node j) and one for the input (component b, node k). The interpolation is done once, inside the integrals that define the matrix. The matrix is upper triangular in the node index by the third property in Eq. (1.5.10). Section 6 constructs it explicitly.

FK tables

A measured quantity is a convolution of distributions at the scale of the measurement with a hard cross-section computed in perturbation theory. For a deep inelastic data point I at (x_I, Q_I^2), discretised in the same way, the prediction is a row vector C_I contracted with the distributions at Q_I. Insert the evolution operator:

$$\begin{aligned} T_I &= \sum_{a,j} C_{I,aj}\; x_j f_a(x_j, Q_I^2) = \sum_{b,k} \mathrm{FK}_{I,bk}\; x_k f_b(x_k, Q_0^2), \\ \mathrm{FK}_{I,bk} &= \sum_{a,j} C_{I,aj}\, E_{aj,bk}(Q_I^2, Q_0^2). \end{aligned} \tag{1.5.12}$$

The array $\mathrm{FK}_{I,bk}$ is the *FK table* for that data point. It is the evolution operator from the fitting scale to the scale of the measurement, already folded with the hard cross-section. For a process with two incoming hadrons the prediction is quadratic in the distributions, and the table carries two pairs of indices. In the NNPDF pipeline the hard cross-sections are stored as PineAPPL grids and the operators are produced by the EKO code; the two are combined into FK tables once per choice of theory [3].

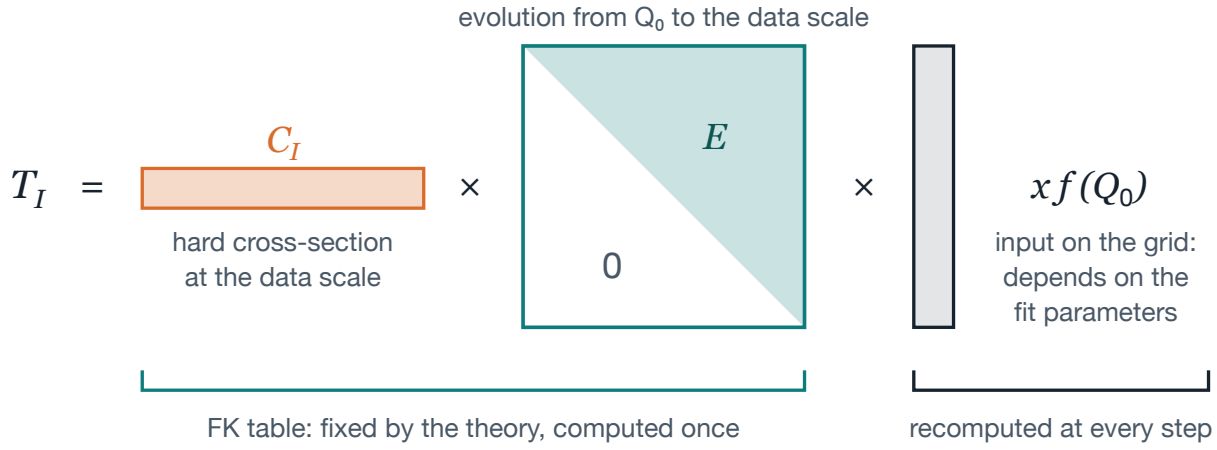

Figure 2. The structure of Eq. (1.5.12). The evolution matrix is triangular because only larger momentum fractions feed a given x. The product of the hard cross-section and the evolution matrix does not involve the fitted parameters, so it is stored. A fit then evaluates one matrix product per prediction.

Why a fit is fast. The fit parameters θ enter a prediction only through the numbers $x_k f_b(x_k, Q_0^2; \theta)$. Everything else in Eq. (1.5.12) is independent of θ. Solving the evolution equations is expensive and is done once. Evaluating a prediction is a product of a stored array with a short vector, and it is repeated for every trial θ. The same product is differentiable in θ, which is what gradient-based samplers and minimisers need. The cost is rigidity: a change of α_S, of the perturbative order or of a quark mass changes E, and every table must be regenerated.

---

4. Moment space at leading order

This section completes the leading-order solution of chapter 1.4: the full singlet solution in closed form, and the numerical step that takes moments back to x.

The singlet solution with projectors

For each moment N the singlet equation (1.4.23) is a pair of ordinary differential equations with the matrix of anomalous dimensions

$$\boldsymbol{\gamma}(N) = \begin{pmatrix} \gamma_{qq} & 2n_f\gamma_{qg} \\ \gamma_{gq} & \gamma_{gg} \end{pmatrix},$$

whose entries are given in Eq. (1.4.26) and whose eigenvalues $\gamma_\pm(N)$ are given in Eq. (1.4.29). At leading order this matrix does not depend on the scale. Changing variable from t to ζ, exactly as for Eq. (1.4.28), gives $d\mathbf{q}/d\zeta = \boldsymbol{\gamma}\,\mathbf{q}/2\pi b$ with constant coefficients, where $\mathbf{q} = (\Sigma, g)^T$ and $b = (33 - 2n_f)/12\pi$. The solution is a matrix exponential. Written with the projectors onto the two eigenvectors (derivation D2):

$$\begin{pmatrix} \Sigma(N,\mu^2) \\ g(N,\mu^2) \end{pmatrix} = \left[\mathsf{P}_+ \, e^{d_+\zeta} + \mathsf{P}_- \, e^{d_-\zeta} \right] \begin{pmatrix} \Sigma(N,\mu_0^2) \\ g(N,\mu_0^2) \end{pmatrix}, \qquad d_\pm(N) = \frac{\gamma_\pm(N)}{2\pi b}, \tag{1.5.13}$$

$$\mathsf{P}_\pm = \pm\,\frac{\boldsymbol{\gamma} - \gamma_\mp \mathbb{1}}{\gamma_+ - \gamma_-}, \qquad \mathsf{P}_\pm^2 = \mathsf{P}_\pm, \quad \mathsf{P}_+\mathsf{P}_- = 0, \quad \mathsf{P}_+ + \mathsf{P}_- = \mathbb{1}. \tag{1.5.14}$$

Since $e^\zeta = \alpha_S(\mu_0^2)/\alpha_S(\mu^2)$, each term is a power of the ratio of couplings, as in the non-singlet case. No eigenvectors need to be found: the projectors are built from the matrix itself.

The second moment as an example. At $N = 2$, Eq. (1.4.26) gives $\boldsymbol{\gamma} = \begin{pmatrix} -\frac{16}{9} & \frac{n_f}{3} \\ \frac{16}{9} & -\frac{n_f}{3} \end{pmatrix}$ with $\gamma_+ = 0$ and $\gamma_- = -(\frac{16}{9} + \frac{n_f}{3})$. Then

$$\mathsf{P}_+ = \frac{1}{16 + 3n_f} \begin{pmatrix} 3n_f & 3n_f \\ 16 & 16 \end{pmatrix}.$$

Acting on $(\Sigma, g)^T$ this gives $(\Sigma + g)$ times the vector $(3n_f, 16)/(16 + 3n_f)$. The part of the solution that does not decay is the total momentum, shared between quarks and gluons in the asymptotic ratio of Eq. (1.4.30). The other projector multiplies a term that decays as $e^{d_-\zeta}$.

Back to x: the inverse Mellin transform

The moments determine the distribution through the inverse transform

$$x\,f(x) = \frac{1}{2\pi i}\int_{c-i\infty}^{c+i\infty} dN\; x^{1-N}\, f(N),$$

where the contour runs parallel to the imaginary axis, to the right of every singularity of $f(N)$ (ESW Eq. 4.134). Except in special cases the integral must be done numerically.

Where the singularities are. There are two sources. The anomalous dimensions have poles on the real axis: γ_{gg} and γ_{gq} at $N = 1$, and all four at $N = 0$ and at negative integers. The input has its own: if $xf(x) \sim x^a$ at small x, the moment integral diverges for $N \le 1 - a$, and $f(N)$ has a pole at $N = 1 - a$. A valence-like input with $a = \frac{1}{2}$ has its rightmost pole at $N = \frac{1}{2}$. A sea or gluon input that rises at small x like $x^{-0.2}$ has it at $N = 1.2$, to the right of the pole of γ_{gg}. All of these lie on the real axis.

Choosing the contour. On the straight line $N = c + i\tau$ the factor x^{1-N} only oscillates, and the integral converges slowly. Because every singularity is on the real axis, the contour can be bent towards the negative real direction without crossing any. On the bent contour x^{-N} decays exponentially for $x < 1$. Using $f(N^*) = f(N)^*$ to fold the lower half onto the upper (derivation D6):

$$\begin{aligned} x\,f(x) &= \frac{1}{\pi}\int_0^\infty d\tau\; \mathrm{Im}\Big[e^{i\phi}\, x^{1-N(\tau)}\, f\big(N(\tau)\big)\Big], \\ N(\tau) &= c + \tau\, e^{i\phi}, \qquad \tfrac{\pi}{2} < \phi < \pi. \end{aligned} \tag{1.5.15}$$

The check script uses $c = 1.8$ and $\phi = 3\pi/4$. It reproduces the input distributions to one part in 10^8, and gives the same answer with $c = 1.2$, $\phi = 0.6\pi$, as Cauchy's theorem requires.

Anomalous dimensions at complex N. The contour needs $\gamma_{ab}(N)$ for complex N, but Eq. (1.4.26) contains the harmonic sum $\sum_{k=1}^{N} 1/k$, which is defined only for integers. The sum entered through an integral that makes sense for any N (derivation D5 of chapter 1.4), and that integral is the digamma function ψ:

$$H_N \equiv \sum_{k=1}^{N}\frac{1}{k} = \int_0^1 dx\,\frac{1-x^N}{1-x} = \psi(N+1) + \gamma_E, \tag{1.5.16}$$

with $\gamma_E = 0.5772\ldots$ Euler's constant. The right-hand side is analytic for $\mathrm{Re}\,N > -1$ and has poles at the negative integers. Replacing the sum by it in Eq. (1.4.26) gives the anomalous dimensions everywhere on the contour. At higher orders more elaborate sums appear, and each needs its own continuation; this is the main technical cost of working in moment space.

---

5. Beyond leading order in moment space

This section states how the solution changes at next-to-leading order (NLO), derives the non-singlet case in full, and explains why two correct NLO codes can give slightly different numbers.

The coupling at two loops

Beyond leading order the coupling obeys (ESW chapter 2; chapter 1.6, section 2, derives the solution and discusses it)

$$\frac{d\alpha_S}{d\ln\mu^2} = -b\,\alpha_S^2\left(1 + b'\alpha_S + \dots\right), \qquad b' = \frac{153 - 19n_f}{2\pi\,(33 - 2n_f)}. \tag{1.5.17}$$

For $n_f = 4$, $b' = 0.490$; for $n_f = 5$, $b' = 0.401$. Keeping the first two terms, the equation separates. With $\int d\alpha/[\alpha^2(1 + b'\alpha)] = -1/\alpha - b'\ln[\alpha/(1 + b'\alpha)]$, the solution between two scales is

$$\left[\frac{1}{\alpha_S} + b'\ln\frac{\alpha_S}{1 + b'\alpha_S}\right]_{\mu_0}^{\mu} = b\,\ln\frac{\mu^2}{\mu_0^2}. \tag{1.5.18}$$

This is an implicit equation for $\alpha_S(\mu^2)$, solved numerically. As a worked example, start from $\alpha_S(M_Z) = 0.118$ at $M_Z = 91.2$ GeV, run with five flavours down to $m_b = 4.92$ GeV, the bottom mass in the theory used here, and with four flavours from there to $Q_0 = 1.65$ GeV. Equation (1.5.18) gives $\alpha_S(m_b) = 0.213$ and $\alpha_S(Q_0) = 0.327$. With the one-loop formula the same input gives 0.204 and 0.289. The coupling at the starting scale of our fits is large, and the order at which it is run changes it by more than 10% there.

The non-singlet solution at NLO

With the kernel expanded as in Eq. (1.4.34), a non-singlet moment obeys $\partial q/\partial\ln\mu^2 = \frac{\alpha_S}{2\pi}\left[\gamma^{(0)} + \frac{\alpha_S}{2\pi}\gamma^{(1)}\right]q$, where $\gamma^{(1)}(N)$ is the moment of $P^{(1)\pm}$. Divide by Eq. (1.5.17) to use α_S as the variable. The result has a simple exact form (derivation D4):

$$\frac{dq}{d\alpha_S} = -\left[\frac{R_0}{\alpha_S} + \frac{R_1}{1 + b'\alpha_S}\right]q, \qquad R_0 = \frac{\gamma^{(0)}}{2\pi b}, \quad R_1 = \frac{1}{2\pi b}\left[\frac{\gamma^{(1)}}{2\pi} - b'\gamma^{(0)}\right]. \tag{1.5.19}$$

R_0 is the leading-order exponent d_{qq} of Eq. (1.4.28). R_1 combines the two NLO effects: the correction to the kernel and the correction to the running of the coupling. Integrating:

$$q(N,\mu^2) = q(N,\mu_0^2)\left[\frac{\alpha_S(\mu_0^2)}{\alpha_S(\mu^2)}\right]^{R_0}\left[\frac{1 + b'\alpha_S(\mu_0^2)}{1 + b'\alpha_S(\mu^2)}\right]^{R_1/b'}. \tag{1.5.20}$$

This is the exact solution of the equations as truncated in Eqs. (1.5.17) and (1.5.19). It is called the *iterated* solution, because it is what a step-by-step numerical integration of those equations converges to. But the equations themselves are only known to relative order α_S. Expanding the second factor to the same order gives an equally valid answer, the *truncated* solution:

$$q(N,\mu^2) = q(N,\mu_0^2)\left[\frac{\alpha_S(\mu_0^2)}{\alpha_S(\mu^2)}\right]^{R_0}\Big[1 + R_1\big(\alpha_S(\mu_0^2) - \alpha_S(\mu^2)\big)\Big]. \tag{1.5.21}$$

The two differ by terms of relative order α_S^2, which is the size of the next-to-next-to-leading-order correction that neither includes.

Numbers. The check script computes $\gamma^{(1)-}(N)$ for $n_f = 4$ by integrating ESW's Eqs. (4.107), (4.108) and (4.119) numerically. It confirms that the first moment vanishes, which is quark-number conservation at this order (ESW Eq. 4.115). For $N = 2$ it finds $\gamma^{(1)-} = -8.91$, against $\gamma^{(0)} = -1.78$. Evolving the second moment of a valence distribution from $Q_0 = 1.65$ GeV to m_b with the couplings above:

	LEADING ORDER	NLO ITERATED, EQ. (1.5.20)	NLO TRUNCATED, EQ. (1.5.21)
$N = 2$	0.8328	0.8219	0.8204
$N = 8$	0.5838	0.5734	0.5719

The entries are $q(N, m_b^2)/q(N, Q_0^2)$, all three columns using the same two-loop couplings. The NLO terms change the result by 1.3% at $N = 2$ and 1.8% at $N = 8$. The two NLO solutions differ from each other by 0.2 to 0.3%. Neither is wrong. The difference is a part of the uncertainty from missing higher orders, and it shrinks at each order. It also means that two evolution codes can only be compared digit by digit if they use the same solution method.

The singlet at NLO

For the singlet, R_0 and R_1 are 2×2 matrices that do not commute, and the step from Eq. (1.5.19) to Eq. (1.5.20) fails: the exponential of a sum of non-commuting matrices is not the product of the exponentials. The standard remedy [4] is to look for a solution as the leading-order one dressed by a matrix series in the coupling. Expanding $R_1/(1 + b'\alpha_S)$ to lowest order, the equation is $d\mathbf{q}/d\alpha_S = -\alpha_S^{-1}\big[R_0 + \alpha_S R_1\big]\mathbf{q}$, and the ansatz is

$$\begin{aligned} \mathbf{q}(\alpha_S) &= U(\alpha_S)\left[\frac{\alpha_{S0}}{\alpha_S}\right]^{R_0} U^{-1}(\alpha_{S0})\;\mathbf{q}(\alpha_{S0}), \\ U &= 1 + \alpha_S\, U_1 + \ldots, \qquad U_1 + [R_0, U_1] = -R_1. \end{aligned} \tag{1.5.22}$$

Here $\alpha_{S0} = \alpha_S(\mu_0^2)$, the middle factor is the leading-order solution (1.5.13), and the condition on U_1 comes from requiring the equation to hold at first order in α_S (derivation D4). With the projectors of Eq. (1.5.14) and $r_\pm = \gamma_\pm^{(0)}/2\pi b$, the condition is solved by $U_1 = -\sum_{i,j=\pm} \mathsf{P}_i R_1 \mathsf{P}_j/(1 + r_i - r_j)$. For a non-singlet the commutator vanishes, $U_1 = -R_1$, and expanding $U(\alpha_S)U^{-1}(\alpha_{S0})$ to first order reproduces Eq. (1.5.21).

The same freedom appears here. One can expand $U(\alpha_S)U^{-1}(\alpha_{S0})$ to first order (truncated), keep the product as it stands, or integrate the differential equation numerically (iterated). All are NLO solutions. The check script confirms with random matrices that Eq. (1.5.22) agrees with a direct numerical integration up to terms of second order in the coupling.

---

6. Solving in x space

This section builds the evolution matrix directly on a grid in x, with no transform, and compares the result with the moment-space solution.

The convolution on a grid

It is convenient to evolve the momentum density $F(x) = x\,f(x)$, which is finite and smooth where f itself is steep. Multiplying the convolution (1.4.19) by x and substituting $\xi = x/z$:

$$x\,(P \otimes f)(x) = \int_x^1 dz\; P(z)\; F\!\left(\frac{x}{z}\right). \tag{1.5.23}$$

Every leading-order kernel in Eq. (1.4.21) has the form $P(z) = A(z)/(1-z)_+ + B(z) + C\,\delta(1-z)$ with A and B smooth on the range of integration. For P_{qq}, for example, $A = C_F(1+z^2)$, $B = 0$ and $C = \frac{3}{2}C_F$.

The plus distribution was defined in Eq. (1.4.13) by an integral from 0 to 1. Here the integral starts at x. Applying the definition to a function that vanishes below x gives (derivation D3)

$$\int_x^1 dz\,\frac{g(z)}{(1-z)_+} = \int_x^1 dz\,\frac{g(z)-g(1)}{1-z} + g(1)\,\ln(1-x). \tag{1.5.24}$$

The logarithm is the part of the virtual subtraction that comes from $0 < z < x$, where there is no real emission to set against it. It is negative, and it grows without limit as $x \to 1$: close to $x = 1$ a quark can only lose momentum.

Now insert the interpolation (1.5.11) for F and evaluate Eq. (1.5.23) at the node x_i. With $g(z) = A(z)F(x_i/z)$, so that $g(1) = A(1)F_i$, the result is a matrix acting on the vector of node values $F_j = F(x_j)$ (derivation D3):

$$\begin{aligned} x_i\,(P\otimes f)(x_i) &= \sum_j K_{ij}\,F_j, \\ K_{ij} &= \int_{x_i}^1 dz\left[\frac{A(z)\,w_j(x_i/z) - A(1)\,\delta_{ij}}{1-z} + B(z)\,w_j\Big(\frac{x_i}{z}\Big)\right] \\ &\quad + \delta_{ij}\Big[A(1)\ln(1-x_i) + C\Big]. \end{aligned} \tag{1.5.25}$$

Three features of K:

- **The integrand is finite at $z = 1$.** There $w_j(x_i/z) \to w_j(x_i) = \delta_{ij}$, so the numerator of the first term vanishes. The cancellation between real and virtual emission has been built into each matrix element.
- **K is upper triangular.** The argument x_i/z is never below x_i, so only nodes $j \geq i$ contribute.
- **K depends only on the grid and the kernel.** It is computed once by ordinary quadrature.

Stepping in the scale

The evolution equations are now a system of ordinary differential equations for the node values:

$$\frac{d\mathbf{F}}{d\ln\mu^2} = \frac{\alpha_S(\mu^2)}{2\pi}\,K\,\mathbf{F}, \qquad \text{so at leading order} \qquad \mathbf{F}(Q^2) = \exp\Big[\frac{\zeta}{2\pi b}\,K\Big]\mathbf{F}(Q_0^2). \tag{1.5.26}$$

For a non-singlet $\mathbf{F}$ has n entries and K is the matrix for P_{qq}. For the singlet $\mathbf{F}$ has $2n$ entries and K is built from four blocks, arranged as in Eq. (1.4.23). The matrix exponential in Eq. (1.5.26) is the discretised evolution operator of section 3. It exists in closed form only at leading order, where the change of variable to ζ removes the scale dependence of the coefficient.

In general the system is integrated numerically in steps of $\ln\mu^2$. The simplest rule is Euler's: $\mathbf{F}(t+h) = \mathbf{F}(t) + h\,\frac{\alpha_S}{2\pi}K\,\mathbf{F}(t)$, with an error per unit t proportional to h. The fourth-order Runge–Kutta rule evaluates the right-hand side four times per step and has an error proportional to h^4. To propagate the operator itself, integrate with the identity matrix as the starting value.

The two solvers compared

The check script implements Eqs. (1.5.25) and (1.5.26) and the moment-space solution of section 4, and runs both on the toy input of chapter 1.4 with $n_f = 4$ and $\Lambda = 0.2$ GeV. The grid has 240 intervals: 80 equal steps in $\ln x$ from 10^{-5} to 0.1 and 160 equal steps in x from 0.1 to 1. The interpolating functions w_k are linear in $\ln x$ between neighbouring nodes.

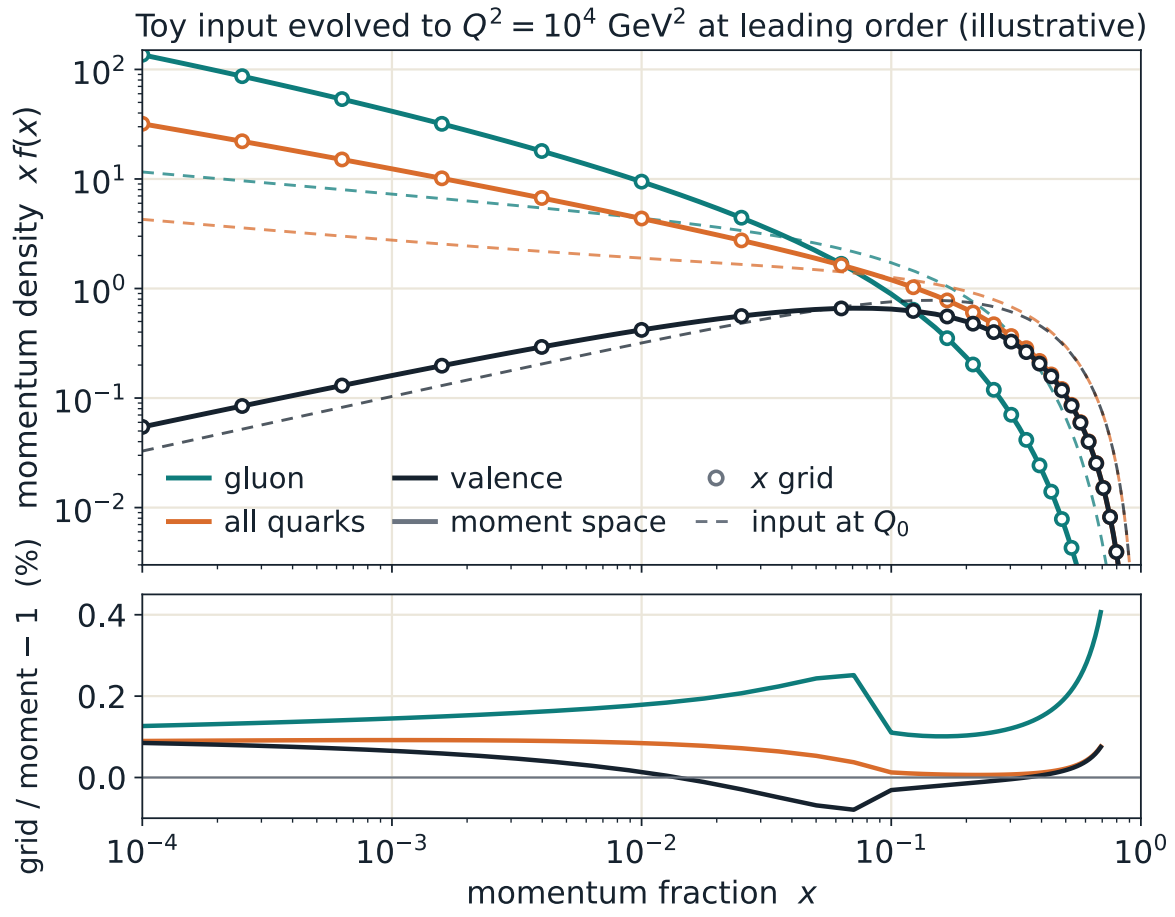

Figure 3. Two independent solutions of the leading-order equations. Upper panel: the toy input at $Q_0 = 1.65$ GeV (dashed) and its evolution to $Q^2 = 10^4$ GeV^2, from the moment-space solution of Eqs. (1.4.28) and (1.5.13) (lines) and from the x-space matrix of Eq. (1.5.26) on 240 intervals (circles). Lower panel: their relative difference; the step at $x = 0.1$ is where the grid spacing changes. The inputs are illustrative, not a fit.

The largest relative differences between the two solvers at $Q^2 = 10^4$ GeV^2, over $10^{-4} < x < 0.7$, are:

GRID	VALENCE	SINGLET	GLUON
240 intervals	0.08%	0.09%	0.37%
480 intervals	0.02%	0.03%	0.11%

Halving the spacing reduces the difference by a factor of 3.5, close to the factor of 4 expected of linear interpolation, whose error is proportional to the square of the spacing. So the difference is the discretisation error of the grid method, and the two solvers converge to the same answer. The gluon is worst at large x, where it falls steeply and straight-line interpolation is poorest. Production codes use higher-order interpolating polynomials and reach much smaller errors on fewer nodes.

For the step in scale, with the grid fixed: Runge–Kutta with 20 steps between Q_0^2 and 10^4 GeV^2 reproduces the matrix exponential to 3×10^{-7}. Euler with 80 steps is still wrong by 2.8%, and its error halves when the number of steps doubles. As a check on the total, the momentum carried by the grid solution above $x = 10^{-5}$ at $Q^2 = 10^4$ GeV^2 is 0.9941; the moment-space solution puts 0.0074 below that point, so the two account for the full momentum to 0.15%.

The same operator can be applied to a different input. The script evolves a second shape with the matrix computed for the first and again matches the moment-space result. This is the property that FK tables rely on.

Which method

ESW remark that the singlet equations are most easily solved by direct integration in x space, and that higher-order kernels are straightforward to include in either method [1]. Both are in use. Of the public codes listed in the Snowmass report [3], QCD-PEGASUS works in moment space [4], HOPPET in x space [5], APFEL in x space [6], and EKO computes its operators in moment space and delivers them on an x grid [7].

	MOMENT SPACE	x SPACE
The convolution	a product, exact	a matrix, with interpolation error
Leading-order solution	closed form	matrix exponential or stepping
Input needed	moments, or a transform of the input	values on the grid
Main difficulty	continuing the kernels to complex N; the inversion integral	the plus distribution; grid density at large x

7. Heavy-quark thresholds

This section explains how the equations change when the scale passes a quark mass, and what the choices are for the charm distribution.

The number of flavours depends on the scale

Everything so far assumed n_f massless flavours. The number enters in four places: the coefficient b of the running coupling, the term $-\frac{2}{3}n_f T_R$ in γ_{gg}, the factor $2n_f$ multiplying P_{qg} in the singlet equation, and the list of non-singlet combinations. A quark of mass m_h cannot be produced by gluons of virtuality far below m_h^2, so at scales $\mu \ll m_h$ it should not be counted. At $\mu \gg m_h$ its mass is negligible and it behaves like any other flavour.

A *variable-flavour-number scheme* makes this a rule. The scale axis is divided at the charm, bottom and top masses. Between two thresholds the equations are solved with a fixed n_f: three below m_c, four between m_c and m_b, five above m_b. At each threshold the solution with n_f flavours is converted into the starting condition for $n_f + 1$. The evolution operator across a threshold is a product, by the composition rule of Eq. (1.5.10):

$$E(Q^2, Q_0^2) = E^{(5)}(Q^2, m_b^2)\ \mathsf{A}_b\ E^{(4)}(m_b^2, Q_0^2), \qquad m_c < Q_0 < m_b < Q. \tag{1.5.27}$$

A_b is the matching at the bottom threshold, described next.

Matching the coupling and the distributions

The coupling. In the $\overline{\text{MS}}$ scheme, with the matching done at $\mu = m_h$, the coupling is continuous across the threshold at leading and next-to-leading order. Its slope is not: b falls from $25/12\pi = 0.663$ to $23/12\pi = 0.610$ on passing from four to five flavours, so the coupling runs more slowly above. From next-to-next-to-leading order the coupling itself has a small step at the threshold.

The distributions. The distributions for $n_f + 1$ flavours are related to those for n_f by a convolution with calculable matching functions:

$$f_i^{(n_f+1)}(x,m_h^2) = \sum_j \left(\mathsf{A}_{ij} \otimes f_j^{(n_f)}\right)(x,m_h^2),$$
$$\mathsf{A}_{ij}(z) = \delta_{ij}\,\delta(1-z) + \left(\frac{\alpha_S}{2\pi}\right)^2 \mathsf{A}_{ij}^{(2)}(z) + \dots \tag{1.5.28}$$

The first non-trivial term at $\mu = m_h$ is of order α_S^2 [3, 8]. The term of order α_S is proportional to $\ln(\mu^2/m_h^2)$ and vanishes when the matching is done at the mass. So at leading and next-to-leading order the light distributions are continuous and the heavy quark starts from zero. At next-to-next-to-leading order, the order of our fits, the light distributions have small discontinuities and the heavy quark starts from a small non-zero value.

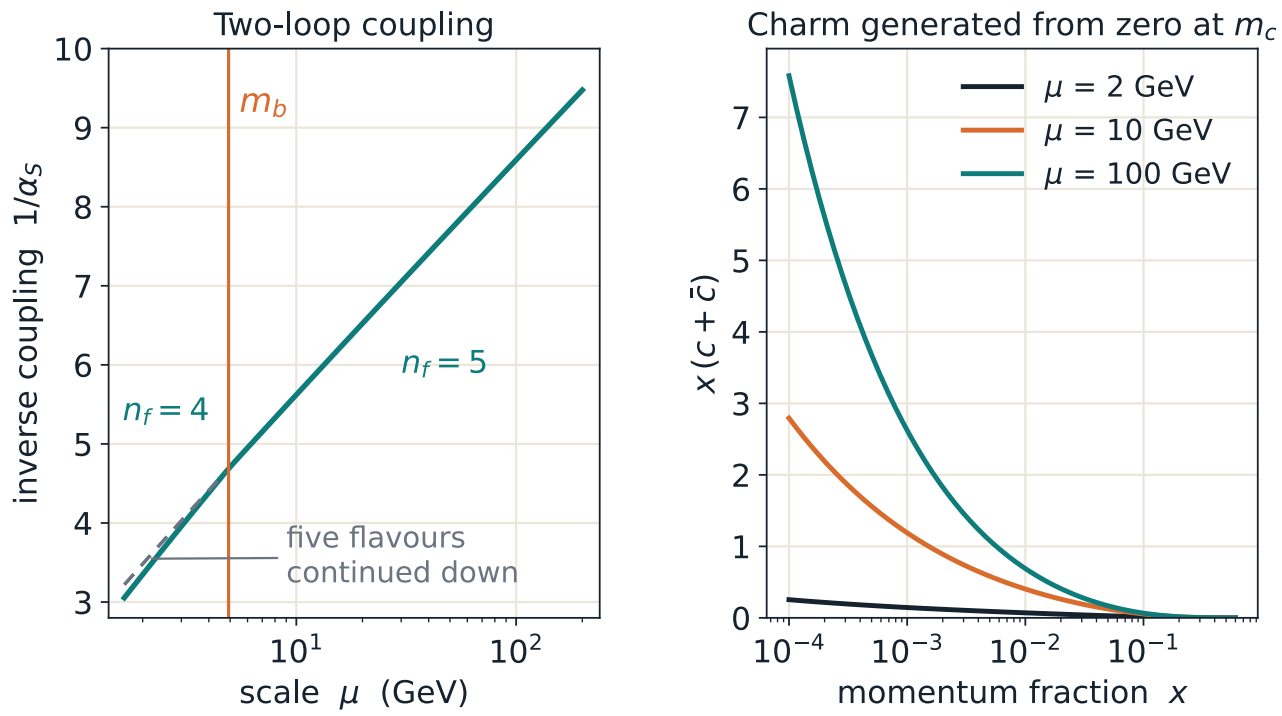

Figure 4. Two effects of a threshold. Left: $1/\alpha_S$ from Eq. (1.5.18) with $\alpha_S(M_Z) = 0.118$ and the bottom threshold at $m_b = 4.92$ GeV. The curve is continuous with a change of slope; the dashed line continues the five-flavour running below the threshold. Right: charm generated by leading-order evolution from zero at $m_c = 1.51$ GeV, for the toy input of Figure 3 placed at m_c (illustrative).

Charm generated by radiation

Above m_c the first line of Eq. (1.5.3) applies to charm. At leading order,

$$\frac{\partial c^+}{\partial \ln \mu^2} = \frac{\alpha_S}{2\pi}\Big[P_{qq} \otimes c^+ + 2P_{qg} \otimes g\Big].$$

The gluon term is a source that does not need any charm to be present. Starting from $c^+(x, m_c^2) = 0$ and working to first order in α_S:

$$c^+(x,\mu^2) \;\approx\; \frac{\alpha_S}{2\pi}\,\ln\frac{\mu^2}{m_c^2}\,2\,\big(P_{qg} \otimes g\big)(x). \tag{1.5.29}$$

Charm obtained this way is called *perturbative* or *radiatively generated*. It is fixed by the gluon and the charm mass, with no free parameter.

In the evolution basis nothing special has to be done. At the threshold $T_{15} = \Sigma$, by section 2. Above it, Σ evolves with the gluon in the singlet system while T_{15} evolves alone, so they separate, and $c^+ = (\Sigma - T_{15})/4$ is whatever the difference has grown to. Figure 4 (right) is computed in exactly this way. For the toy input, the momentum carried by $c + \bar{c}$ grows from zero at m_c to 1.2% at 3 GeV, 2.4% at 10 GeV and 3.8% at 100 GeV. The check script confirms Eq. (1.5.29) just above the threshold.

Fitted charm, and what our fits do

The alternative is to give charm its own parametrised distribution at the starting scale and let the data determine it. This allows for a non-perturbative, or *intrinsic*, charm component of the proton. NNPDF4.0 fits charm in this way, while the other global fits generate it perturbatively, and the Snowmass report records that in dedicated fits the fitted charm at the initial scale carries between 0 and 1% of the proton's momentum, depending on the settings [3].

The theory used in this project is of the fitted-charm type: theory 40000000 has the flag `IC = 1`, with $m_c = 1.51$ GeV and $Q_0 = 1.65$ GeV (Phase B ledger). The starting scale is above the charm mass, so evolution upward from Q_0 runs with at least four flavours and the charm distribution at Q_0 is an input. Our MSHT20-form model sets that input to zero. The ledger records this as a deliberate hybrid: a theory that allows fitted charm, used with a parametrisation that has none. Charm in our predictions is therefore generated by evolution from zero at Q_0. At leading order that is Eq. (1.5.29) with m_c replaced by Q_0.

Mass effects near threshold

Treating a heavy quark as massless above its threshold is accurate only for $Q^2 \gg m_h^2$. Near the threshold the hard cross-section depends on m_h^2/Q^2. *General-mass* schemes keep that dependence in the coefficient functions while still summing the logarithms of Q^2/m_h^2 through evolution. Our theory uses one of them, FONLL-C. This is a statement about coefficient functions, not about the evolution of the distributions, and it is taken up in chapter 1.6.

---

8. Large x

This section derives how the fall-off of a quark distribution near $x = 1$ steepens with the scale.

Parametrisations build in a power-law fall-off, $f \sim (1-x)^{\beta}$ as $x \to 1$ (Moore, section 1.2.4 [2]). The exponent cannot stay fixed under evolution. Large x corresponds to large N, because x^{N-1} is concentrated near $x = 1$. There the non-singlet anomalous dimension is dominated by the harmonic sum, $H_N \to \ln N + \gamma_E$:

$$\gamma_{qq}(N) = C_F\Big[\frac{3}{2} - 2\ln N - 2\gamma_E\Big] + O\Big(\frac{1}{N}\Big). \tag{1.5.30}$$

The logarithm is the moment-space image of the $1/(1-x)_+$ in P_{qq}: it comes from soft gluon emission.

Suppose that at μ_0 a non-singlet distribution behaves as $A\,(1-x)^{\beta_0}$ near $x = 1$. Its high moments are $A\,\Gamma(\beta_0 + 1)\,N^{-(\beta_0+1)}$. Under Eq. (1.4.28) the $-2C_F \ln N$ in Eq. (1.5.30) multiplies them by a further power of N, which is a further power of $(1-x)$. The result is (derivation D5)

$$\begin{aligned} q(x,\mu^2) \;&\xrightarrow{x\to 1}\; A\; e^{(\frac{3}{4}-\gamma_E)\Delta}\;\frac{\Gamma(\beta_0+1)}{\Gamma(\beta_0+1+\Delta)}\;(1-x)^{\beta_0+\Delta}, \\ \Delta &= \frac{C_F}{\pi b}\,\zeta = \frac{C_F}{\pi b}\ln\frac{\alpha_S(\mu_0^2)}{\alpha_S(\mu^2)}. \end{aligned} \tag{1.5.31}$$

The exponent grows linearly in ζ, that is, like $\ln\ln\mu^2$ (ESW Eq. 4.137). The prefactor, which ESW do not give, follows from the constant terms in Eq. (1.5.30).

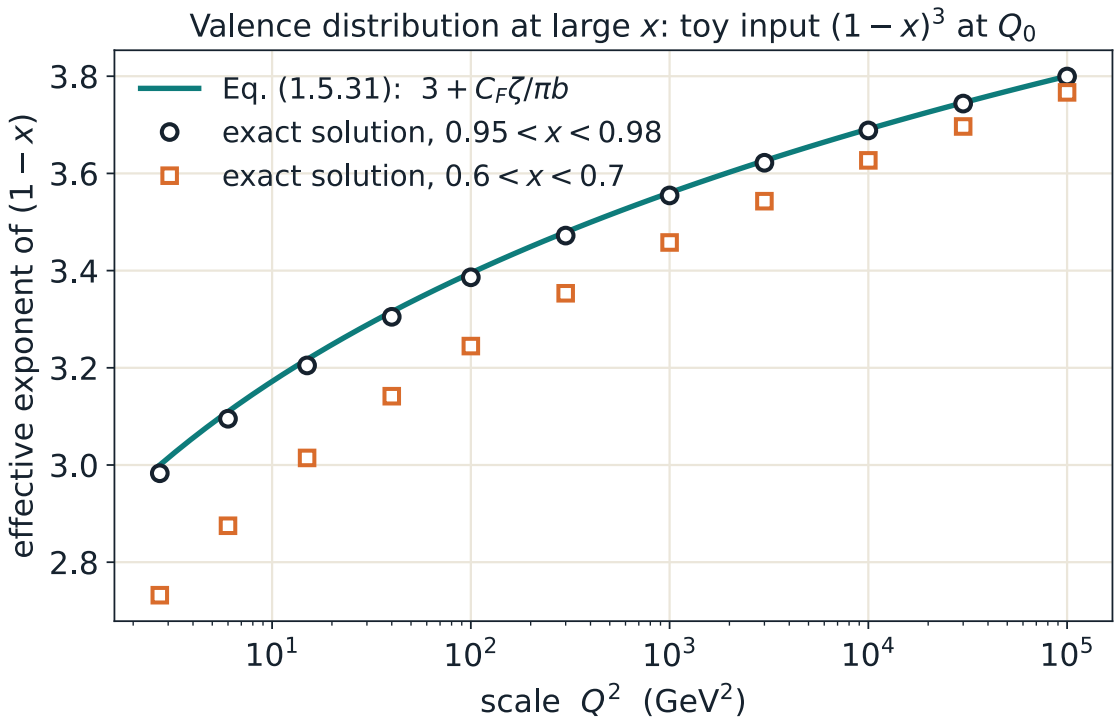

Figure 5. The exponent of $(1-x)$ in the valence momentum density. Line: Eq. (1.5.31) with $n_f = 4$, $\Lambda = 0.2$ GeV and $\beta_0 = 3$. Circles: the logarithmic slope of the exact leading-order solution between $x = 0.95$ and 0.98. Squares: the same slope measured between $x = 0.6$ and 0.7, where the asymptotic form does not yet apply. The input is the toy valence shape (illustrative).

Numbers. For $n_f = 4$, $C_F/\pi b = 16/25$. From $Q_0 = 1.65$ GeV to $Q^2 = 10^4$ GeV^2 with the toy coupling, $\zeta = 1.08$ and $\Delta = 0.69$: an input $(1-x)^3$ becomes $(1-x)^{3.69}$. The exact solution has slope 3.69 between $x = 0.95$ and 0.98, and the normalisation in Eq. (1.5.31) agrees with it to 2% at $x = 0.98$.

Three consequences.

- **A large-x exponent is tied to a scale.** The parameters β of a functional form describe the distribution at Q_0 only. Quoting an exponent without its scale is incomplete.
- **The gluon is steeper still.** At large x the gluon is fed by the quarks through $P_{gq} \otimes q$. That integral runs over a range of width $1-x$, which supplies one more power: a quark distribution $\propto (1-x)^\beta$ generates a gluon $\propto (1-x)^{\beta+1}$.
- **The formula is asymptotic.** Figure 5 shows that between $x = 0.6$ and 0.7 the local slope lies below the line, by about 0.3 at Q_0, because the factor $x^{1/2}$ of the input still matters there. Corrections are of relative order $1-x$.

The same soft-gluon logarithms appear in coefficient functions as $x \to 1$, where they can be summed to all orders (threshold resummation [3]). Fixed-order fits, including ours, do not include that resummation.

---

9. Small x

This section places the double-logarithmic result of chapter 1.4 in context and states where fixed-order evolution is expected to fail.

What the starting distributions look like

Before perturbative evolution acts, the behaviour at small x is taken from Regge theory, which relates $x \to 0$ at fixed Q^2 to the high-energy limit of hadron scattering. It suggests $x\,g$ and $x\,\Sigma$ roughly constant and valence distributions behaving as $x^{-1/2}$ at a hadronic scale of order 1 GeV (ESW section 4.6.1; Moore, Eq. 1.96 [2]). This is the origin of the factor x^{α} in every parametrisation.

Evolution then steepens the gluon and the sea. Equation (1.4.32) gives the asymptotic form when the input is flat. If the input is already steep, $x\,g \sim x^{-\lambda}$, its moments have a pole at $N = 1 + \lambda$. When that pole lies to the right of the saddle point of derivation D6 in chapter 1.4, it controls the inversion integral, and the input power survives the evolution (ESW section 4.6.2). In the toy solution of Figure 3, with input $x^{-0.2}$, the effective power of the gluon between $x = 10^{-5}$ and 10^{-6} is 0.32 at $Q^2 = 100$ GeV^2 and 0.40 at 10^4 GeV^2.

Logarithms of $1/x$ in the kernels

The double-logarithmic estimate kept only the $1/x$ term of the leading-order P_{gg}. Higher orders bring more powers of $\ln(1/x)$. For each of the four singlet kernels (ESW Eq. 4.187),

$$x\,P(x,\alpha_S) = \sum_{n=0}^{\infty} \left(\frac{\alpha_S}{2\pi}\right)^n \left[\sum_{m=0}^{n} A_m^{(n)}\, \ln^m \frac{1}{x} + x\,\overline{P}^{(n)}(x)\right], \tag{1.5.32}$$

with $\overline{P}^{(n)}$ finite as $x \to 0$. The overall factor $\alpha_S/2\pi$ of the evolution equation is not included, so the term n belongs to order α_S^{n+1}. Each order can bring one more logarithm. The approximations are then:

APPROXIMATION	TERMS OF EQ. (1.5.32) KEPT
Leading-order DGLAP	$n = 0$, all of it
Double logarithms, Eq. (1.4.32)	$A_0^{(0)}$ only
NLO DGLAP	$n = 0, 1$, all of both
Leading logarithms of $1/x$	$m = n$ for every n

For P_{gg} the leading coefficients are $A_0^{(0)} = 2C_A = 6$, then $A_1^{(1)} = A_2^{(2)} = 0$, then $A_3^{(3)} = 2\zeta(3)(2C_A)^4/3! \approx 519$ (ESW Eq. 4.188 prints 518.4 without a formula; that number is this expression with $\zeta(3)$ rounded to 1.2, which is our inference). Only P_{gg} and P_{gq} have such leading terms at all.

DGLAP and BFKL

The DGLAP equation sums powers of $\alpha_S \ln Q^2$ from emissions strongly ordered in transverse momentum, Eq. (1.4.33). When $\ln(1/x)$ is large and $\ln Q^2$ is not, a different set of terms dominates: powers of $\alpha_S \ln(1/x)$, from emissions ordered in momentum fraction with no ordering in transverse momentum. Summing those is the task of the Balitsky–Fadin–Kuraev–Lipatov (BFKL) equation [9], which is an evolution equation in $\ln(1/x)$ at fixed transverse momentum. Its leading-order solution for fixed coupling is a power (ESW Eq. 4.189):

$$x\,g(x) \sim x^{-\lambda}, \qquad \lambda = \frac{12\ln 2}{\pi}\,\alpha_S = 4\ln 2\,\frac{C_A\alpha_S}{\pi} \;\approx\; 0.5 \quad \text{for } \alpha_S \approx 0.19. \tag{1.5.33}$$

This is steeper than the double-logarithmic growth, which is slower than any power.

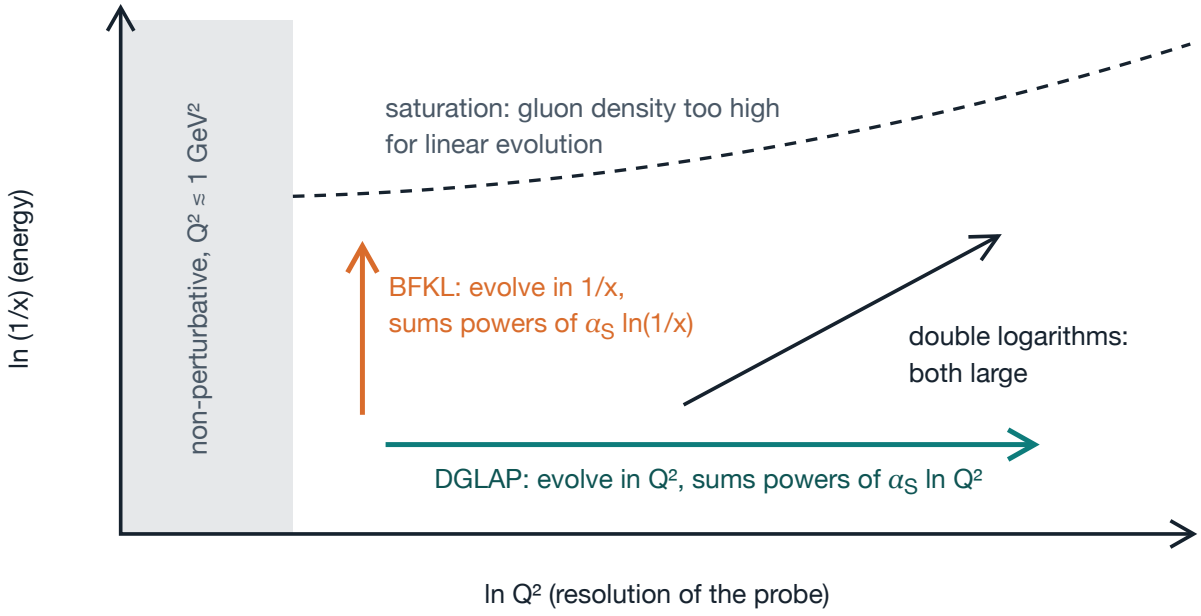

Figure 6. The regimes of evolution, after ESW Fig. 4.18. DGLAP evolution moves a known distribution to the right. BFKL evolution moves it upward. Along the diagonal both logarithms are large and the two descriptions share the double-logarithmic terms. Above the dashed line the gluon density is so high that gluons recombine, and no linear equation applies. The positions of the boundaries are schematic.

Where fixed-order DGLAP is trusted

A naive criterion would be $\alpha_S \ln(1/x) \ll 1$. That fails early: with the toy coupling at $Q^2 = 100\ \text{GeV}^2$ the product $\alpha_S \ln(1/x)$ is already 2.2 at $x = 10^{-5}$. Yet NLO fits described the HERA data at small x well (ESW section 4.6.1). Three facts from the sources explain the situation and its limits.

- **The first two leading logarithms are absent.** $A_1^{(1)} = A_2^{(2)} = 0$ in P_{gg}, so the leading logarithms of $1/x$ first enter the gluon kernel at the fourth order in α_S. Fixed-order evolution at NLO and NNLO is not driven by them.
- **Subleading terms are large.** The Snowmass report notes that the subleading small-x terms are found to be larger than the leading ones, so that several towers of logarithms would have to be summed for quantitative control [3]. ESW add that the leading-logarithm kernels do not conserve momentum [1].
- **There is evidence of the breakdown in data.** A global fit with small-x resummation [10] found significant evidence for it in the HERA structure-function data at small x and low Q^2, and forward measurements at the LHC reach $x \sim 10^{-6}$ [3].

In practice fixed-order DGLAP is used wherever data exist, and its predictions are treated with caution at the smallest x and lowest Q^2. The fixed-target deep inelastic data that anchor our Phase A fits lie at $x \gtrsim 0.01$ (ESW section 4.4), far from this region.

---

10. Accuracy, and where our fits use this

How accurate evolution has to be, and is

The numerical solution of the evolution equations is not a source of physical uncertainty. It is a discretisation error, and it can be reduced at will by a finer grid, a better interpolation or more steps. The requirement is only that it be far below the experimental errors, which are at the per-cent level for the best data.

The standard test is the one carried out in section 6: solve the same equations by two unrelated methods and compare. With the elementary methods of this chapter the agreement is 0.1% on 480 intervals, improving as the square of the spacing. Two statements from the sources set this in context.

- ESW, writing when distributions were distributed as fitted analytic formulas, quote an accuracy at the per-cent level for such formulas against the exact numerical solution [1].
- The Snowmass report lists several public programs that solve the equations at NNLO, describes present NNLO distributions as having benchmarked accuracy, and notes that it took more than ten years from the publication of the NNLO kernels to reach that point [3]. Neither source quotes a number of digits, so none is quoted here.

Section 5 adds a caution. At NLO and beyond, two codes agree digit by digit only if they solve the truncated equations in the same way. The difference between the iterated and truncated solutions, 0.2 to 0.3% in the example there, is not a numerical error. It belongs with the uncertainty from missing higher orders.

In this project

- **The basis.** Colibri models return their distributions in the fourteen-component evolution basis, and our runcards set the basis to `EVOL` (Phase B ledger). The 52 parameters of the MSHT20 form describe the distributions at $Q_0 = 1.65$ GeV, and the model hands them to the FK tables in this basis.
- **Unfilled components are a physics statement.** A grid model that populated only Σ, g and V reached $\chi^2/N_{\text{dat}} = 8.02$ on 648 points of proton and deuteron data (PPDF-8). The FK contraction multiplied real sensitivity to T_3 by zero, and Eq. (1.5.8) shows why that is fatal for a proton–deuteron difference. Populating V_3, T_3 and T_8 as well gave 5.84 (PPDF-9).
- **Evolution is frozen into the tables.** Theory 40000000 fixes NNLO evolution, $\alpha_S(M_Z) = 0.118$, $Q_0 = 1.65$ GeV, $m_c = 1.51$ GeV and the FONLL-C scheme. Phase A and Phase B use the same theory, so differences between their results cannot come from evolution.
- **Charm.** The theory allows fitted charm; our parametrisation sets charm to zero at Q_0 (section 7). The effect of that choice has not been measured: the comparison planned for it, PPDF-30b, is recorded in the ledger as not run.

Derivations

D1. Decoupling of the non-singlet combinations

Derives (1.5.3), (1.5.5)

The general equations. For n_f flavours the evolution equations are (ESW Eq. 4.90)

$$\frac{\partial q_i}{\partial t} = \frac{\alpha_S}{2\pi}\Big[\sum_k \left(P_{q_i q_k} \otimes q_k + P_{q_i \bar{q}_k} \otimes \bar{q}_k\right) + P_{qg} \otimes g\Big],$$

and the same with $q \leftrightarrow \bar{q}$ throughout for $\bar{q}_i$. The gluon kernel P_{qg} is the same for every flavour and for quark and antiquark, Eq. (1.4.23).

Insert the flavour structure. With Eq. (1.5.2) the sum over k splits into a term with $k = i$ and a term that sums over all flavours:

$$\frac{2\pi}{\alpha_S}\frac{\partial q_i}{\partial t} = P_{qq}^V \otimes q_i + P_{q\bar q}^V \otimes \bar q_i + P_{qq}^S \otimes \sum_k q_k + P_{q\bar q}^S \otimes \sum_k \bar q_k + P_{qg} \otimes g,$$
$$\frac{2\pi}{\alpha_S}\frac{\partial \bar q_i}{\partial t} = P_{qq}^V \otimes \bar q_i + P_{q\bar q}^V \otimes q_i + P_{qq}^S \otimes \sum_k \bar q_k + P_{q\bar q}^S \otimes \sum_k q_k + P_{qg} \otimes g.$$

Add and subtract. In the sum, $\sum_k (q_k + \bar q_k) = \Sigma$ appears with coefficient $P_{qq}^S + P_{q\bar q}^S$, and the gluon term doubles. In the difference, $\sum_k (q_k - \bar q_k) = V$ appears with coefficient $P_{qq}^S - P_{q\bar q}^S$, and the gluon term cancels. With $P^{\pm} = P_{qq}^V \pm P_{q\bar q}^V$ these are the two lines of Eq. (1.5.3).

Differences of flavours. For two flavours i and j, subtract the first line of Eq. (1.5.3) for j from that for i. The Σ and g terms are identical and cancel:

$$\frac{\partial}{\partial t}\left(q_i^+ - q_j^+\right) = \frac{\alpha_S}{2\pi}\, P^+ \otimes \left(q_i^+ - q_j^+\right).$$

Each T in Eq. (1.5.4) is a combination of such differences. For example $T_8 = (u^+ - s^+) + (d^+ - s^+)$, and in general the coefficients in each row of Eq. (1.5.4) sum to zero. Since the equation is linear, every T_j obeys it. The same argument with the second line gives the equation for the V_j with kernel P^-.

The two sums. Summing the second line of Eq. (1.5.3) over the n_f flavours gives $\partial V/\partial t = \frac{\alpha_S}{2\pi}\left[P^- + n_f(P_{qq}^S - P_{q\bar q}^S)\right] \otimes V$, which defines P^V. Summing the first line gives

$$\frac{\partial \Sigma}{\partial t} = \frac{\alpha_S}{2\pi}\Big[\left(P^+ + n_f(P_{qq}^S + P_{q\bar q}^S)\right) \otimes \Sigma + 2n_f\, P_{qg} \otimes g\Big],$$

the upper row of Eq. (1.4.23). The gluon equation involves the quarks only through $\sum_k (P_{gq} \otimes q_k + P_{gq} \otimes \bar q_k) = P_{gq} \otimes \Sigma$. So Σ and g form a closed pair, and Eq. (1.5.5) is complete.

Check. In moment space each kernel is a number. The check script fills the 7×7 evolution matrix for three flavours and the gluon with random values of the seven independent kernels, rotates it with R of Eq. (1.5.6), and finds exactly the pattern above: a 2×2 block for (Σ, g), diagonal entries P^V, P^-, P^-, P^+, P^+, and zeros elsewhere.

D2. The matrix exponential from projectors

Derives (1.5.13), (1.5.14)

Let M be a 2×2 matrix with distinct eigenvalues λ_+ and λ_-, and define

$$\mathsf{P}_+ = \frac{M - \lambda_- 1}{\lambda_+ - \lambda_-}, \qquad \mathsf{P}_- = \frac{\lambda_+ 1 - M}{\lambda_+ - \lambda_-}.$$

Three identities. Adding the two definitions, $\mathsf{P}_+ + \mathsf{P}_- = 1$. Taking $\lambda_+\mathsf{P}_+ + \lambda_-\mathsf{P}_-$, the terms in 1 cancel and the result is M. The product is

$$\mathsf{P}_+\mathsf{P}_- = -\frac{(M - \lambda_- 1)(M - \lambda_+ 1)}{(\lambda_+ - \lambda_-)^2} = 0,$$

because a matrix satisfies its own characteristic equation (the Cayley–Hamilton theorem). Then $\mathsf{P}_+^2 = \mathsf{P}_+(1 - \mathsf{P}_-) = \mathsf{P}_+$, and likewise for P_-.

Powers and the exponential. From $M = \lambda_+\mathsf{P}_+ + \lambda_-\mathsf{P}_-$ and the identities, the cross terms vanish in every power: $M^k = \lambda_+^k\mathsf{P}_+ + \lambda_-^k\mathsf{P}_-$. Summing the exponential series term by term,

$$e^{sM} = e^{s\lambda_+}\,\mathsf{P}_+ + e^{s\lambda_-}\,\mathsf{P}_-.$$

Application. At leading order the singlet moments obey $d\mathbf{q}/d\zeta = \boldsymbol{\gamma}\,\mathbf{q}/2\pi b$ with a constant matrix, so $\mathbf{q}(\zeta) = \exp[\zeta\boldsymbol{\gamma}/2\pi b]\,\mathbf{q}(0)$. Setting $M = \boldsymbol{\gamma}$ and $s = \zeta/2\pi b$ gives Eqs. (1.5.13) and (1.5.14). The composition rule of Eq. (1.5.10) is the statement $e^{(s_1+s_2)M} = e^{s_2 M}e^{s_1 M}$.

Why this fails beyond leading order. If the matrix depends on the evolution variable, the solution is $\exp[\int M\,ds]$ only when the matrices at different s commute. At NLO the matrix is $R_0 + \alpha_S R_1$ and $[R_0, R_1] \neq 0$.

The check script compares Eq. (1.5.13) with a general-purpose matrix exponential at a complex value of N and finds agreement to machine precision.

D3. The plus distribution on a grid

Derives (1.5.24), (1.5.25)

A restricted range. Let $g(z)$ be smooth on $x \le z \le 1$. Apply the definition (1.4.13) to the function equal to $g(z)$ for $z > x$ and zero for $z < x$. Its value at $z = 1$ is $g(1)$, so

$$\int_x^1 dz\,\frac{g(z)}{(1-z)_+} = \int_0^1 dz\,\frac{g(z)\,\theta(z-x) - g(1)}{1-z} = \int_x^1 dz\,\frac{g(z)-g(1)}{1-z} - g(1)\int_0^x \frac{dz}{1-z}.$$

The last integral is $-\ln(1-x)$, which gives Eq. (1.5.24).

The convolution. Write the kernel as $P(z) = A(z)/(1-z)_+ + B(z) + C\,\delta(1-z)$. In Eq. (1.5.23) the delta function gives $C\,F(x)$. The B term is an ordinary integral. For the plus term use Eq. (1.5.24) with $g(z) = A(z)\,F(x/z)$ and $g(1) = A(1)\,F(x)$:

$$x\,(P\otimes f)(x) = \int_x^1 dz\left[\frac{A(z)\,F(x/z) - A(1)\,F(x)}{1-z} + B(z)\,F\!\left(\frac{x}{z}\right)\right] + \Big[A(1)\ln(1-x) + C\Big]F(x).$$

Interpolate. Set $x = x_i$ and replace $F(y)$ by $\sum_j w_j(y)F_j$ from Eq. (1.5.11). Then $F(x_i/z) = \sum_j w_j(x_i/z)F_j$ and $F(x_i) = F_i = \sum_j \delta_{ij}F_j$. Collecting the coefficient of F_j gives K_{ij} of Eq. (1.5.25).

The integrand near $z = 1$. For linear interpolation in $\ln y$ between x_i and x_{i+1}, the weight of node i at the point $y = x_i/z$ is $w_i = 1 + \ln z/h_i$ with $h_i = \ln(x_{i+1}/x_i)$. As $z \to 1$, $\ln z \to -(1-z)$, so $[A(z)w_i - A(1)]/(1-z) \to -A'(1) - A(1)/h_i$, which is finite. The weight of node $i+1$ is $-\ln z/h_i$, which is itself proportional to $1-z$. No singular integral has to be evaluated.

Triangularity. $w_j(x_i/z)$ is non-zero only if x_i/z lies within one interval of x_j. Since $x_i/z \ge x_i$, this needs $j \ge i$.

Check. For $F(y) = y^{1/2}(1-y)^3$ the script compares $\sum_j K_{ij}F_j$ for P_{qq} with the convolution evaluated directly by adaptive quadrature, at four values of x between 3×10^{-5} and 0.78, and finds agreement to 0.2% or better on the 240-interval grid.

D4. The next-to-leading-order solution

Derives (1.5.19), (1.5.20), (1.5.21), (1.5.22)

The equation in α_S. A non-singlet moment obeys $dq/dt = \frac{\alpha_S}{2\pi}\big[\gamma^{(0)} + \frac{\alpha_S}{2\pi}\gamma^{(1)}\big]q$ and the coupling obeys $d\alpha_S/dt = -b\,\alpha_S^2(1 + b'\alpha_S)$. Dividing,

$$\frac{dq}{d\alpha_S} = -\frac{\gamma^{(0)} + \frac{\alpha_S}{2\pi}\gamma^{(1)}}{2\pi b\,\alpha_S\,(1 + b'\alpha_S)}\;q.$$

Partial fractions. With R_0 and R_1 as defined in Eq. (1.5.19), $\gamma^{(0)}/2\pi b = R_0$ and $\gamma^{(1)}/4\pi^2 b = R_1 + b'R_0$. The numerator divided by $2\pi b$ is then $R_0 + \alpha_S(R_1 + b'R_0) = R_0(1 + b'\alpha_S) + \alpha_S R_1$, so

$$\frac{dq}{d\alpha_S} = -\left[\frac{R_0}{\alpha_S} + \frac{R_1}{1 + b'\alpha_S}\right] q.$$

This is Eq. (1.5.19), with no approximation beyond the two truncations already made.

Integrate. $\ln q = -R_0 \ln\alpha_S - (R_1/b')\ln(1 + b'\alpha_S) + \text{const}$. Fixing the constant at μ_0 gives Eq. (1.5.20).

Truncate. $\ln\left[(1 + b'\alpha_{S0})/(1 + b'\alpha_S)\right] = b'(\alpha_{S0} - \alpha_S) + O(\alpha_S^2)$, so the second factor in Eq. (1.5.20) is $\exp[R_1(\alpha_{S0} - \alpha_S)]\,(1 + O(\alpha_S^2)) = 1 + R_1(\alpha_{S0} - \alpha_S) + O(\alpha_S^2)$. This is Eq. (1.5.21). The script confirms that the ratio of the two solutions differs from 1 by an amount that falls by a factor of 4 when both couplings are halved.

The matrix case. For the singlet, R_0 and R_1 are matrices. Insert the ansatz of Eq. (1.5.22) into $\alpha_S\, d\mathbf{q}/d\alpha_S = -(R_0 + \alpha_S R_1)\,\mathbf{q}$. Since $\alpha_S \frac{d}{d\alpha_S}\alpha_S^{-R_0} = -R_0\,\alpha_S^{-R_0}$ acts to the right of U, the left side is $\left[\alpha_S U' - U R_0\right] U^{-1}\mathbf{q}$. Multiplying by U from the right:

$$\alpha_S\, U' = U\, R_0 - \left(R_0 + \alpha_S R_1\right) U.$$

At order α_S^0 this reads $0 = R_0 - R_0$. At order α_S^1, with $U = 1 + \alpha_S U_1$: $U_1 = U_1 R_0 - R_0 U_1 - R_1$, which is the condition in Eq. (1.5.22).

Solving for U_1. Sandwich the condition between projectors, $\mathsf{P}_i(\dots)\mathsf{P}_j$, and use $R_0\mathsf{P}_j = r_j\mathsf{P}_j$: $(1 + r_i - r_j)\,\mathsf{P}_i U_1 \mathsf{P}_j = -\mathsf{P}_i R_1 \mathsf{P}_j$. Summing over i, j with $\sum_i \mathsf{P}_i = 1$ gives the expression quoted below Eq. (1.5.22).

D5. The large-x exponent

Derives (1.5.31)

Moments of a power of $(1 - x)$. $\int_0^1 dx\, x^{N-1}(1 - x)^\beta = \Gamma(N)\Gamma(\beta + 1)/\Gamma(N + \beta + 1)$. For large N, $\Gamma(N)/\Gamma(N + \beta + 1) \to N^{-(\beta+1)}$. So a distribution behaving as $A(1 - x)^{\beta_0}$ near $x = 1$ has $q(N, \mu_0^2) \to A\,\Gamma(\beta_0 + 1)\,N^{-(\beta_0+1)}$.

The anomalous dimension. In Eq. (1.4.26), $1/N(N + 1)$ is negligible and $H_N = \ln N + \gamma_E + O(1/N)$, which gives Eq. (1.5.30).

Evolve. By Eq. (1.4.28) the moment is multiplied by $\exp[\gamma_{qq}\zeta/2\pi b]$. With $\Delta = C_F\zeta/\pi b$,

$$\frac{\gamma_{qq}(N)\,\zeta}{2\pi b} = \Delta\left(\frac{3}{4} - \gamma_E\right) - \Delta\ln N, \qquad \text{so} \qquad q(N, \mu^2) \to A\,\Gamma(\beta_0 + 1)\,e^{(\frac{3}{4} - \gamma_E)\Delta}\,N^{-(\beta_0 + 1 + \Delta)}.$$

Invert. Reading the first step backwards, $N^{-(\beta+1)}$ is the large-N moment of $(1 - x)^\beta/\Gamma(\beta + 1)$. With $\beta = \beta_0 + \Delta$ this gives Eq. (1.5.31).

Validity. Each step drops terms of relative order $1/N$, which correspond to relative order $1 - x$ in the distribution. The result is the leading behaviour as $x \to 1$ and nothing more.

D6. The bent contour

Derives (1.5.15)

The inversion formula. With $x = e^{-u}$, the moment $f(N) = \int_0^\infty du\, e^{-(N-1)u}\,[xf(x)]$ is a Laplace transform in u of the function $xf(x)$. The standard inversion of the Laplace transform is $xf(x) = \frac{1}{2\pi i}\int_{c-i\infty}^{c+i\infty} dN\, e^{(N-1)u} f(N)$, with c to the right of all singularities of $f(N)$. Since $e^{(N-1)u} = x^{1-N}$, this is the formula quoted in section 4.

Fold onto the upper half. For a real distribution, $f(N^*) = f(N)^*$, and $x^{1-N^*} = (x^{1-N})^*$. The part of the contour below the real axis is the mirror image of the part above, traversed so that the two contributions are complex conjugates after the factor $1/2\pi i$. Their sum is twice the real part of the upper contribution:

$$x\,f(x) = \frac{1}{\pi}\,\mathrm{Im}\int_{\text{upper}} dN\; x^{1-N} f(N).$$

Bend it. The integrand is analytic away from the real axis. The upper half of the vertical line can be rotated about the point c to the ray $N = c + \tau e^{i\phi}$, $\tau > 0$, with $\frac{\pi}{2} < \phi < \pi$, provided the integrand vanishes on the arc at infinity between the two. It does for $x < 1$: there $\mathrm{Re}\,N \le c$, so $|x^{1-N}|$ is bounded, and $f(N)$ falls as a power of $|N|$. On the ray $dN = e^{i\phi} d\tau$, which gives Eq. (1.5.15).

Why it helps. On the ray, $|x^{1-N}| = x^{1-c}\exp\big[-\tau\,|\cos\phi|\,\ln(1/x)\big]$. The integrand is cut off exponentially at $\tau \sim 1/[|\cos\phi|\ln(1/x)]$. On the vertical line it decays only through $f(N)$. The script evaluates the same inversion both ways and finds the same value to one part in 10^7. The bent contour needs fewer than a thousand evaluations of the integrand with a fixed quadrature rule. The straight one needs an adaptive routine that follows the oscillations out to τ of several thousand.

References

1. R. K. Ellis, W. J. Stirling and B. R. Webber, *QCD and Collider Physics*, Cambridge University Press (1996), chapter 4. Open access under CC BY-NC 4.0, doi:10.1017/CBO9780511628788. Section 2 follows its Eqs. (4.95)–(4.101), section 8 its Eqs. (4.135)–(4.137), section 9 its section 4.6; the next-to-leading-order kernels used in section 5 are its Eqs. (4.107), (4.108) and (4.119). The wording, derivations and figures are our own.
2. J. M. Moore, *Parton Distributions in Beyond the Standard Model Theories*, PhD thesis, University of Cambridge, sections 1.2.1 and 1.2.4.
3. S. Amoroso et al., “Snowmass 2021 whitepaper: Proton structure at the precision frontier”, arXiv:2203.13923. Source for the statements on evolution codes, threshold matching, fitted charm and small-x resummation.
4. A. Vogt, “Efficient evolution of unpolarized and polarized parton distributions with QCD-PEGASUS”, Comput. Phys. Commun. 170 (2005) 65, arXiv:hep-ph/0408244.
5. G. P. Salam and J. Rojo, “A Higher Order Perturbative Parton Evolution Toolkit (HOPPET)”, Comput. Phys. Commun. 180 (2009) 120, arXiv:0804.3755.
6. V. Bertone, S. Carrazza and J. Rojo, “APFEL: A PDF Evolution Library with QED corrections”, Comput. Phys. Commun. 185 (2014) 1647, arXiv:1310.1394.
7. A. Candido, F. Hekhorn and G. Magni, “EKO: evolution kernel operators”, arXiv:2202.02338.
8. M. Buza, Y. Matiounine, J. Smith and W. L. van Neerven, Eur. Phys. J. C 1 (1998) 301, arXiv:hep-ph/9612398.

9. E. A. Kuraev, L. N. Lipatov and V. S. Fadin, Sov. Phys. JETP 44 (1976) 443 and 45 (1977) 199; I. I. Balitsky and L. N. Lipatov, Sov. J. Nucl. Phys. 28 (1978) 822.
10. R. D. Ball, V. Bertone, M. Bonvini, S. Marzani, J. Rojo and L. Rottoli, Eur. Phys. J. C 78 (2018) 321, arXiv:1710.05935.